Supplementary

Participants

The inclusion criteria for participants with mild cognitive impairment (MCI) were as follows: (I) participants diagnosed with MCI at the time of data collection; (II) magnetic resonance imaging (MRI) and ^{18}F-fluorodeoxyglucose positron emission tomography (^{18}F-FDG PET) scans collected for each participant. Participants' data were retrieved from the Alzheimer's Disease Neuroimaging Initiative (ADNI) database (cohort A) and the Department of Neurology at Huashan Hospital in Shanghai, China (cohort B), and participants in both cohorts were categorized into 2 groups: an MCI nonconverter (MCI-nc) group, whose MCI did not convert to Alzheimer's disease (AD), and an MCI-converter (MCI-c) group, whose MCI did convert to AD. Cohort A consisted of 168 MCI-cs and 187 MCI-ncs, while cohort B comprised 10 MCI-cs and 12 MCI-ncs. Cohort A also contained the MRI and ^{18}F-FDG PET data of 94 healthy control participants obtained at 2 points in time with an average interval of 2 years. The inclusion criteria for the healthy control participants were as follows: (I) a Mini-Mental State Examination (MMSE) score of between 24 and 30; (II) a clinical dementia rating (CDR) of 0; (III) and no diagnosis of depressions, MCI, or dementia. This data set was used to perform a stability analysis on the radiomic features.

Cohort B comprised 10 MCI-cs and 12 MCI-ncs. Participants in this cohort had both MRI and ^{18}F-FDG PET imaging data. MCI-ncs remained clinically stable, while MCI-cs converted to Alzheimer's disease (AD) during the average follow-up period of 24.5±9.6 months. MCI was diagnosed according to previously published criteria (1).

Acquisition protocol

ADNI (cohort A)

Detailed information on the structural MRI and ^{18}F-FDG PET data acquisition for cohort A can be obtained by visiting the image protocol column of the ADNI dataset on the official website of the ADNI (http://adni.loni.usc.edu/). For the participants in the present study, ^{18}F-FDG PET images were acquired in a resting state 30-35 minutes after the injection of 185±18.5 MBq FDG.

Huashan Hospital (cohort B)

Structural MRI

MRI data for all participants in cohort B were obtained using a 3T MR750 scanner (General Electric Company, Boston, MA, USA). An inversion recovery prepared fast spoiled gradient recalled sequence was used to obtain T1 weighted, high-resolution, 3-dimensional (3D) anatomical brain images. The scanning range was from the cranial crest to the occipital foramen. The scan parameters were as follows: repetition time (TR) =11.1 ms, echo time (TE) =5.0 ms, flip angle =20°, matrix size =256×256, voxel size = 1×1×1 mm^3, field of view (FOV) =240 mm^2, slice thickness = 1.0 mm; 146 slices without slice gap, and transverse acquisition.

https://dx.doi.org/10.21037/atm-21-4349

^{18}F-FDG PET

A Siemens Biograph 64 HD PET/CT scanner was used to perform ^{18}F-FDG PET scanning in 3D mode at resting state (1.5 min/bed, 5 bed positions). All participants were required to have been fasting for at least 6 hours before the examination. Each participant received an intravenous injection of 185 MBq ±37 FDG and rested in a quiet and dark environment for 45 minutes prior to the scan. Before PET scanning, we used low-dose CT transmission scanning to reduce the effects of attenuation.

Data preprocessing protocol

Data preprocessing for the PET and MRI images was performed using the Statistical Parametric Mapping 12 package (SPM12, the Wellcome Department of Neurology, London U.K.) in MATLAB 2016b (MathWorks Inc., Natick, MA, USA).

First, dcm2nii software (http://www.nitrc.org/projects/dcm2nii/) was used to convert digital imaging and communications in medicine (DICOM) files to neuroimaging informatics technology initiative (NIFTI) files. Second, each original 18F-FDG PET scan was registered to a corresponding original structural MRI scan and corrected for partial volume effect (PVE) using the voxel-wise PVE method. Then, the MRI images were segmented using the unified segmentation method. Next, the forward parameters were estimated during the unified segmentation, and the original MRI scan, gray matter (GM) binary mask, and registered PET image were registered to the Montreal Neurological Institute (MNI) stereotaxic template. Finally, the normalized PET scans were smoothed.

^{18}F-FDG PET: each original structural MRI scan was used to register a corresponding original ^{18}F-FDG PET scan. PVE algorithms were used to correct PVE in the PET scans, using the PETPVE12 toolbox, after a voxel-wise method defined by Muller-Gartner *et al.* (2). Our study-specific settings included the specification of an isotropic PSF of 6 mm. The same transformation parameters were used to normalize the registered PET scan to the MNI template. Finally, an isotropic gaussian kernel of 8 mm was used to smooth the normalized PET scans to increase signal-to-noise ratios. Some of the processing results are shown as examples in Figure S1.

MRI: the unified segmentation method was used to segment MRI images into gray matter (GM), white matter (WM), and cerebrospinal fluid (CSF) tissue probability maps. Then, the original MRI scan and GM binary mask were registered to the MNI stereotaxic template using the forward parameters. Some processing results are shown as examples in Figure S1.

Individual GM binary masks were derived from 50% GM suprathreshold voxels plus those whose GM probability exceeded that of WM and CSF. The final positioning of the brain regions is shown in Figure S2. Individual GM binary masks were used to mask the corresponding normalized MRI, and the smoothed 18F-FDG PET scans in the MNI space.

Feature extraction

Texture features [9 from the gray-level co-occurrence matrix (GLCM), 13 from the gray-level run-length matrix (GLRLM), 13 from the gray-level size zone matrix (GLSZM), and 5 from the neighborhood gray-tone difference matrix (NGTDM)] were used to measure tissue heterogeneity by quantitatively describing the spatial distribution of intensities within the regions of interest (ROIs). The first-order intensity features, including variance, skewness, and kurtosis, were calculated according to the intensity distribution of each ROI. All texture features were calculated using 3D analysis (26 neighborhoods). For each texture matrix, only 1 comprehensive texture matrix was calculated by simultaneously considering the adjacent attributes of voxels in 13 directions of 3D space. At the same time, considering discretization length differences, the 6 voxels at a distance of 1 voxel, the 12 voxels at a distance of $\sqrt{2}$ voxels, and the 8 voxels at a distance of $\sqrt{3}$ voxels around the center voxels were treated differently in the calculation of the matrices (3).

The calculation of the texture matrices was dependent on the gray level quantization values since they quantify the relationship between the levels of gray. A reasonable gray level quantization value shortened the calculation time of the feature matrix and improve the signal-to-noise ratio of the texture outcome. Following previous texture analysis research, we selected the number of gray levels (i.e., the dynamic range) as 32 and 64. Wavelet band-pass filtering highlighted detailed information in images at different spatial frequencies. When performing wavelet band-pass filtering, we first performed

https://dx.doi.org/10.21037/atm-21-4349

wavelet decomposition in ROIs on the images in 8 directions (LLL, LLH, LHL, LHH, HLL, HLH, HHL, and HHH), and then defined a coefficient R, indicating the ratio of the weight applied to band-pass sub-bands (LLH, HLH, LHL, HLL, HHL, and LHH) compared to the weight applied to low-frequency and high-frequency sub-bands (LLL and HHH). By adjusting R, and then performing the inverse wavelet transformation, a transformed ROI image was obtained, emphasizing detailed information at different spatial frequencies. Following previous research (4), we extracted wavelet features at 5 spatial frequencies, with R values of 1/2, 2/3, 1 (without wavelet filtering), 3/2, and 2. After selecting the gray level quantization range and wavelet band-pass filter weight (R), we extracted the same number of first-order intensity features and texture features for the processed image.

Finally, we extracted 430 radiomic features from each ROI for each participant's MRI and 18F-FDG PET data. For participants with both MRI and PET scans, a total of 68,800 features were extracted (430×80×2 =68,800). The most basic features in each ROI included first-order intensity features (n=3) and textural features (n=40). By selecting different feature extraction parameters, more features were obtained. We combined different wavelet filter weights (5 levels) and quantization of gray levels (to 2 levels) to extract the features, with 430 features [(3+40)×5×2 = 430] extracted for each ROI.

Conserved features in different modalities

After removing duplicate features, 16 different conserved features remained. The meanings of these features are as follows: the variance feature extracted from the GLCM category is an indicator of dispersion of the unit values around the mean (5); the coarseness feature extracted from the NGTDM has been likened to granularity within an image—that is, coarseness is higher in images of larger granularity and lower in those with a smaller granularity (6); the contrast and busyness features are both derived from the NGTDM and define local texture features by describing the differences between each voxel and the neighboring voxels. Contrast relates to the difference between neighboring regions of voxel intensities, and high contrast in an image indicates that there is a significant difference in voxel intensity between adjacent voxels. Busyness correlates with the change rate between neighborhood intensities weighted by the difference in intensities, and the characteristic of a busy texture is that the intensity of adjacent voxels changes rapidly (7).

https://dx.doi.org/10.21037/atm-21-4349

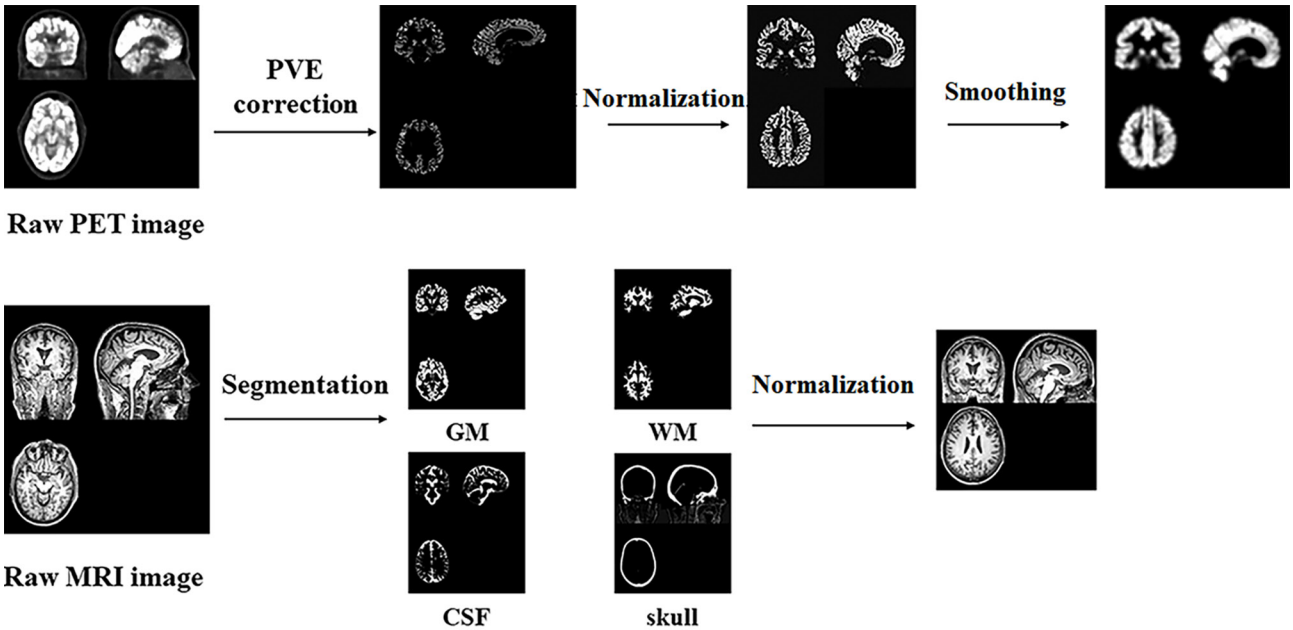

Figure S1 An example of the PET and MRI preprocessing results. PET, positron emission tomography; MRI, magnetic resonance imaging; GM, gray matter; WM, white matter; CSF, cerebrospinal fluid.

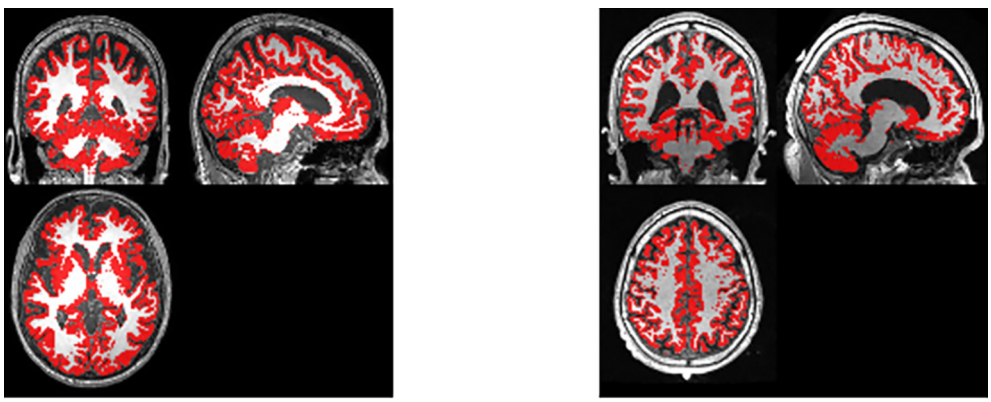

$$((P_{GM} > P_{WM}) \cap (P_{GM} > P_{CSF})) \cup (P_{GM} > 0.5)$$

Figure S2 Final positioning of brain regions. GM, gray matter; WM, white matter; CSF, cerebrospinal fluid.

https://dx.doi.org/10.21037/atm-21-4349

Table S1 Conserved features in the different Cox models

Top	Times	Modality	Labeled number	Labeled region	R	Gray level	Feature name
(a) Single-modality PET model							
1	196	PET	64	SupraMarginal_R	2.00	32	SZHGE
2	194	PET	37	Hippocampus_L	1.50	32	GLV
3	194	PET	39	ParaHippocampal_L	1.00	64	Busyness
4	185	PET	68	Precuneus_R	1.50	64	Correlation
5	181	PET	33	Cingulum_Mid_L	1.50	32	ZP
6	179	PET	33	Cingulum_Mid_L	1.50	32	LZLGE
7	176	PET	67	Precuneus_L	2.00	32	ZSV
8	157	PET	8	Frontal_Mid_R	0.50	32	Skewness
9	144	PET	18	Rolandic_Oper_R	2.00	64	Contrast
10	144	PET	38	Hippocampus_R	1.00	64	Correlation
11	144	PET	68	Precuneus_R	2.00	64	Variance
12	139	PET	34	Cingulum_Mid_R	0.50	64	LZE
13	137	PET	85	Temporal_Mid_L	0.67	64	Contrast
(b) Single-modality MRI model							
1	200	MRI	65	Angular_L	0.50	32	RP
2	198	MRI	39	ParaHippocampal_L	2.00	32	Coarseness
3	196	MRI	90	Temporal_Inf_R	2.00	32	Skewness
4	195	MRI	19	Supp_Motor_Area_L	1.00	64	Strength
5	192	MRI	38	Hippocampus_R	0.50	32	ZP
6	165	MRI	13	Frontal_Inf_Tri_L	0.50	64	Skewness
7	163	MRI	37	Hippocampus_L	1.00	64	Coarseness
8	160	MRI	62	Parietal_Inf_R	1.50	32	Busyness
9	156	MRI	23	Frontal_Sup_Medial_L	0.50	64	Contrast
10	153	MRI	62	Parietal_Inf_R	1.00	64	Skewness
11	147	MRI	21	Olfactory_L	1.50	32	Coarseness
12	134	MRI	38	Hippocampus_R	2.00	32	RLN
(c) Dual-modality model							
1	197	PET	33	Cingulum_Mid_L	1.50	32	ZP
2	191	PET	68	Precuneus_R	1.50	64	Correlation
3	190	MRI	19	Supp_Motor_Area_L	1.00	64	Strength
4	190	MRI	62	Parietal_Inf_R	1.00	64	Skewness
5	188	PET	64	SupraMarginal_R	2.00	32	SZHGE
6	180	PET	67	Precuneus_L	2.00	32	ZSV
7	179	PET	37	Hippocampus_L	1.50	32	GLV
8	174	PET	39	ParaHippocampal_L	1.00	64	Busyness
9	162	PET	34	Cingulum_Mid_R	0.50	64	LZE
10	155	MRI	90	Temporal_Inf_R	2.00	32	Skewness
11	154	PET	52	Occipital_Mid_R	0.50	64	GLN
12	146	PET	39	ParaHippocampal_L	1.00	32	RP
13	146	PET	68	Precuneus_R	2.00	64	Variance
14	138	PET	38	Hippocampus_R	1.00	64	Correlation

Times: the number of times each feature repeated in the 10-fold cross-validation with 200 repetitions of the model construction, R: weights to band-pass subbands in wavelet filtering, gray level: gray level quantization value. SZHGE, small zone high gray-level emphasis; GLV, gray-level variance; ZP, zone percentage; LZLGE, large zone low gray-level emphasis; ZSV, zone-size variance; LZE, large zone emphasis; RP, run percentage; RLN, run-length nonuniformity; GLN, gray-level nonuniformity.

https://dx.doi.org/10.21037/atm-21-4349

Table S2 Crucial image signatures from three image-based models

Top	Modality	Labeled number	Labeled region	R	Gray level	Feature name
1	PET	8	Frontal_Mid_R	0.50	32	Skewness
2	PET	18	Rolandic_Oper_R	2.00	64	Contrast
3	PET	33	Cingulum_Mid_L	1.50	32	ZP
4	PET	33	Cingulum_Mid_L	1.50	32	LZLGE
5	PET	34	Cingulum_Mid_R	0.50	64	LZE
6	PET	37	Hippocampus_L	1.50	32	GLV
7	PET	38	Hippocampus_R	1.00	64	Correlation
8	PET	39	ParaHippocampal_L	1.00	32	RP
9	PET	39	ParaHippocampal_L	1.00	64	Busyness
10	PET	52	Occipital_Mid_R	0.50	64	GLN
11	PET	64	SupraMarginal_R	2.00	32	SZHGE
12	PET	67	Precuneus_L	2.00	32	ZSV
13	PET	68	Precuneus_R	1.50	64	Correlation
14	PET	68	Precuneus_R	2.00	64	Variance
15	PET	85	Temporal_Mid_L	0.67	64	Contrast
16	MRI	13	Frontal_Inf_Tri_L	0.50	64	Skewness
17	MRI	19	Supp_Motor_Area_L	1.00	64	Strength
18	MRI	21	Olfactory_L	1.50	32	Coarseness
19	MRI	23	Frontal_Sup_Medial_L	0.50	64	Contrast
20	MRI	37	Hippocampus_L	1.00	64	Coarseness
21	MRI	38	Hippocampus_R	0.50	32	ZP
22	MRI	38	Hippocampus_R	2.00	32	RLN
23	MRI	39	ParaHippocampal_L	2.00	32	Coarseness
24	MRI	62	Parietal_Inf_R	1.00	64	Skewness
25	MRI	62	Parietal_Inf_R	1.50	32	Busyness
26	MRI	65	Angular_L	0.50	32	RP
27	MRI	90	Temporal_Inf_R	2.00	32	Skewness

Times: the number of times each feature repeated in the 10-fold cross-validation with 200 repetitions of the model construction, R: weights to band-pass subbands in wavelet filtering, gray level: gray level quantization value. ZP, zone percentage; LZLGE, large zone low gray-level emphasis; LZE, large-zone emphasis; GLV, gray-level variance; RP, run percentage; GLN, gray-level nonuniformity; SZHGE, small zone high gray-level emphasis; ZSV, zone-size variance; RLN, run-length nonuniformity.

https://dx.doi.org/10.21037/atm-21-4349

References

1. Dubois B, Feldman HH, Jacova C, et al. Advancing research diagnostic criteria for Alzheimer's disease: the IWG-2 criteria. Lancet Neurol 2014;13:614-29.
2. Müller-Gärtner HW, Links JM, Prince JL, et al. Measurement of radiotracer concentration in brain gray matter using positron emission tomography: MRI-based correction for partial volume effects. J Cereb Blood Flow Metab 1992;12:571-83.
3. Vallières M, Freeman CR, Skamene SR, et al. A radiomics model from joint FDG-PET and MRI texture features for the prediction of lung metastases in soft-tissue sarcomas of the extremities. Phys Med Biol 2015;60:5471-96.
4. Li Y, Jiang J, Lu J, et al. Radiomics: a novel feature extraction method for brain neuron degeneration disease using 18F-FDG PET imaging and its implementation for Alzheimer's disease and mild cognitive impairment. Ther Adv Neurol Disord 2019;12:1756286419838682.
5. Pantic I, Jeremic R, Dacic S, et al. Gray-Level Co-Occurrence Matrix Analysis of Granule Neurons of the Hippocampal Dentate Gyrus Following Cortical Injury. Microsc Microanal 2020;26:166-72.
6. Cheng NM, Fang YH, Chang JT, et al. Textural features of pretreatment 18F-FDG PET/CT images: prognostic significance in patients with advanced T-stage oropharyngeal squamous cell carcinoma. J Nucl Med 2013;54:1703-9.
7. Ahn HK, Lee H, Kim SG, et al. Pre-treatment 18F-FDG PET-based radiomics predict survival in resected non-small cell lung cancer. Clin Radiol 2019;74:467-73.

https://dx.doi.org/10.21037/atm-21-4349